Letters

Free-Positioning Wireless Power Transfer System Based on One-to-Multiple Topology

Jing Chen, Hong Zhou, *Member, IEEE*, Qijun Deng, Fengwei Chen, Ao Zhu, Jiangtao Liu, and Xingran Gao

***Abstract*—The wireless power transfer (WPT) system is an interesting alternative for charging electric vehicles and has a broad prospect in public transport applications. In order to obtain optimal power transfer, the existing WPT systems often require perfect alignment between the primary and secondary coils, which can hardly be met in real applications. To relieve this problem and achieve the goal of free positioning, a one-to-multiple WPT topology being able to improve the misalignment tolerance at the secondary side is proposed in this letter. Based on circuit analysis and MATLAB simulation, a mixed mode is proposed to obtain a steady power transfer with horizontal misalignment. To verify the proposed topology, a one-to-two WPT system with a three winding transformer is developed in this letter, showing that proposed topology with the mixed mode can significantly increase the positioning adaptability.**

***Index Terms*—Free positioning, high-misalignment tolerance, multiple secondary coils, one-to-multiple topology, mixed mode, wireless power transfer (WPT).**

I. Introduction

RECENTLY, wireless power transfer (WPT) has received increased academic attention [1], [2], and has already been employed in many applications, such as the wireless charging of electric vehicles (EVs) [3] and high-speed trains [4], due to its merits of convenience, safety, and reliability. For EVs and rail vehicles (RVs) applications, perfect alignment between the primary coil and secondary coils is usually a prerequisite to guarantee the rated output power as there is only one primary coil and one secondary coil [5], [6]. This makes it necessary to equip a precision positioning maneuver from the driver or an electromechanic alignment system for the secondary coil, making the positioning more difficult. However, to achieve the goal of free positioning, it is necessary to have high-misalignment tolerance between coils as much as possible. To this end, Villa *et al.* [7] proposed a series–parallel–series topology to obtain high-misalignment tolerance. However, it was shown that the misalignment was only increased by 25%. To further improve the misalignment tolerance, another option is to set multiple self-resonators and increase the driving frequency of up to megahertz [8], but this does not conform the wireless charging standards for EVs, i.e., the SAE J2954. Moreover, in the multiple self-resonators topology, there are some dead zones, and thus, free positioning is not always guaranteed.

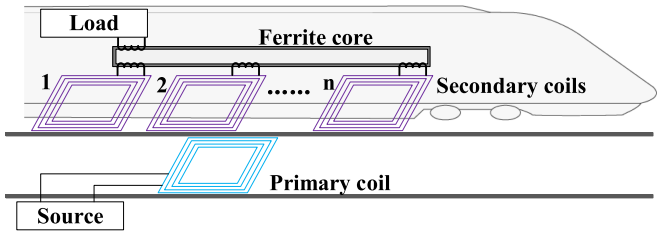

Fig. 1. Schematic diagram of the coupled coil of the proposed WPT system.

In order to alleviate the problem mentioned above, multiple coils can be used on the secondary side. On the one hand, the manufacturing process and installation of primary coil is usually difficult as it needs to be exposed to the outdoors for a long time. Compared to the multiple-to-one topology, the one-to-multiple topology can reduce the manufacturing cost and installation difficulty by the protection of the vehicle body. On the other hand, using multiple small coils can also facilitate the coil design in scenarios where space constraints of the vehicle chassis are one of the major considerations. For a common WPT system with multiple secondary loops, power integration is implemented with the parallel rectifier bridges [9]. However, the output current of each rectifier bridge will be unbalanced due to the inconsistent induced voltages of each secondary loop and the clamping effect of the rectifier diodes. Therefore, this letter focuses on the one-to-multiple WPT topology that supports the free positioning of EVs and RVs.

The topology consists of a primary coil, multiple secondary coils, and a multiwinding transformer, as shown in Fig. 1. Secondary coils are placed side by side on the same plane. The

Manuscript received December 26, 2019; revised January 30, 2020; accepted February 18, 2020. Date of publication February 28, 2020; date of current version June 23, 2020. This work was supported by the National Natural Science Foundation of China under Grant 51677139, Grant 51907054, Grant 51977151, and Grant 61703311. *(Corresponding authors: Qijun Deng; Fengwei Chen.)*

The authors are with the Department of Automation, Wuhan University, Wuhan 430072, China, and also with the Wuhan University Shenzhen Research Institute, Shenzhen 518057, China (e-mail: drchen@whu.edu.cn; hzhouwuhee@whu.edu.cn; dqj@whu.edu.cn; fengwei.chen@whu.edu.cn; zhuao1994@whu.edu.cn; liu_jiangtao@whu.edu.cn; gaoxran@foxmail.com).

Color versions of one or more of the figures in this article are available online at http://ieeexplore.ieee.org.

Digital Object Identifier 10.1109/TPEL.2020.2977199

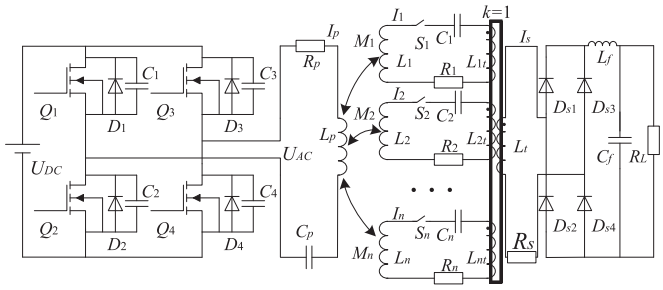

Fig. 2. Equivalent loop of the proposed WPT system.

advantage of using multiple small coils in parallel is that the corresponding secondary coils can be selectively switched ON for power delivery and others can be turned OFF to reduce loop losses, based on the current parking position of the vehicle. The multiwinding transformer can linearly superimpose the energy of each secondary circuit to the load.

In the remainder of this letter, in order to find the relationship between load voltage and coil alignment based on the proposed one-to-multiple WPT topology, an equivalent circuit model was used for theoretical analysis. Subsequently, these theoretical results are validated based on a simulation example, as well as a one-to-two laboratory prototype. Finally, conclusions are drawn in the end.

II. Analytical Modeling

Fig. 2 depicts the equivalent circuit of the proposed system. The primary side includes an inverter, and a resonant loop consisting of a coil L_p and a compensation capacitor C_p. The secondary side includes n resonant loops, where L_i and C_i, $i = 1, 2, \ldots, n$, denote the coils and capacitors, respectively. The power of all secondary loops is assembled by an ideal multiwinding transformer with a ferrite core and subsequently fed to the rectifier, where $L_t, L_{1t}, \ldots, L_{nt}$ are windings of the same design parameters. R_p, R_s, $R_1, \ldots, R_n$ are the parasitic resistances; R_L is the load; U_{DC} is a dc source; U_{AC} is the root-mean-squared (rms) of the ac output voltage of the inverter; $S_1, \ldots, S_n$ are the switches of each secondary loop; I_p, I_s, $I_1, \ldots, I_n$ are the currents of each loop, respectively. The mutual inductances between the primary coil and each secondary coil are denoted as $M_1, \ldots, M_n$, respectively. C_f and L_f are the filter capacitor and filter inductor after the rectifier. In the case where the coils are placed side by side, the mutual inductance is small enough compared with the mutual inductances between primary coil and each secondary coil, so the mutual inductances between the secondary coils are not considered in the following circuit theory-based modeling [10]. Additionally, suppose that the primary loop and secondary loops have the same self-resonant frequency.

A. Analysis of the Ideal Multiwinding Transformer

A multiwinding high-frequency transformer is employed to integrate power from various WPT secondary sides, as shown in Fig. 2. Assuming there is a three windings transformer with primary and secondary inductances $L_{1t} = L_{2t} = L_t$. M_{12} denotes the mutual inductance between the two primary windings, $M_{1\,s}$ and $M_{2\,s}$ are the mutual inductances between the primary winding and secondary windings, respectively. According to the properties of ideal transformers, the flux linkage equation can be expressed as

$$\begin{aligned}\Psi_1 &= L_{1t} \cdot I_1 + M_{12} \cdot I_2 + M_{1\,s} \cdot I_s \\ \Psi_2 &= L_{2t} \cdot I_2 + M_{12} \cdot I_1 + M_{2\,s} \cdot I_s \\ \Psi_s &= L_t \cdot I_s + M_{1\,s} \cdot I_1 + M_{2\,s} \cdot I_2 \end{aligned} \tag{1}$$

where Ψ_1, Ψ_2, and Ψ_s are the flux linkage, respectively. Based on the assumption of an ideal transformer, one can obtain $M_{12} = M_{1\,s} = M_{2\,s} = k\sqrt{L_t L_t} = L_t$. According to (1), the voltage–current equations are

$$\begin{aligned} U_1 = U_2 = U_s &= \frac{\mathrm{d}\Psi_1}{\mathrm{d}t} = \frac{\mathrm{d}\Psi_2}{\mathrm{d}t} = \frac{\mathrm{d}\Psi_s}{\mathrm{d}t} \\ &= L_t \left(\frac{\mathrm{d}I_1}{\mathrm{d}t} + \frac{\mathrm{d}I_2}{\mathrm{d}t} + \frac{\mathrm{d}I_s}{\mathrm{d}t} \right) \end{aligned} \tag{2}$$

where U_1, U_2, and U_s are the induced voltages of each winding, respectively.

By the power conservation law, obviously there is $U_1 \cdot I_1 + U_2 \cdot I_2 = U_s \cdot I_s$, so the currents satisfy $I_1 + I_2 = I_s$. Furthermore, in a multiwinding transformer with n windings, the following relations hold:

$$\begin{aligned} U_1 = U_2 = \cdots = U_n = U_s \\ I_1 + I_2 + \cdots + I_n = I_s. \end{aligned} \tag{3}$$

B. Circuit Analysis of the Proposed System

Based on Kirchhoff's laws, the loop equations can be obtained from Fig. 2

$$\begin{aligned} cU_{\mathrm{AC}} = I_p \cdot Z_p + I_1 \cdot j\omega M_1 + I_2 \cdot j\omega M_2 + \cdots + I_n \cdot j\omega M_n \\ I_p \cdot j\omega M_1 + I_1 \cdot Z_1 + U_1 = 0 \\ \cdots \\ I_p \cdot j\omega M_n + I_n \cdot Z_n + U_n = 0 \\ U_s + I_s \cdot Z_{n+1} = 0 \end{aligned} \tag{4}$$

where $Z_p, Z_1, \ldots, Z_{n+1}$ are impedances of each loop, namely

$$\begin{aligned} Z_p &= R_p + j\omega L_p + \frac{1}{j\omega C_p} \\ Z_1 &= R_1 + j\omega L_1 + \frac{1}{j\omega C_1} \\ &\cdots \\ Z_n &= R_n + j\omega L_n + \frac{1}{j\omega C_n} \\ Z_{n+1} &= R_s + \frac{8}{\pi^2} R_L. \end{aligned} \tag{5}$$

Based on (3), the general solution ($n \geq 2$ and $k \in (1, n)$) of (4) is

$$I_p = \frac{U_{\mathrm{AC}} \left(\sum_{i=1}^{n+1} \prod_{j=1, j\neq i}^{n+1} Z_j \right)}{Q}$$

$$I_k = \frac{-j\omega U_{\mathrm{AC}} \begin{pmatrix} \sum_{i=1, i\neq k}^{n+1} \left(M_k \cdot \prod_{j=1, j\neq k, j\neq i}^{n+1} Z_j \right) \\ -\sum_{i=1, i\neq k}^{n} \left(M_i \cdot \prod_{j=1, j\neq k, j\neq i,}^{n+1} Z_j \right) \end{pmatrix}}{Q}$$

$$I_s = \sum_{i=1}^{n} I_i = \frac{-j\omega U_{\mathrm{AC}} \cdot \sum_{i=1}^{n} \left(M_i \cdot \prod_{j=1, j\neq i}^{n} Z_j \right)}{Q}$$

$$U_s = I_s \cdot \frac{8}{\pi^2} R_L = \frac{-j\omega U_{\mathrm{AC}} \cdot \frac{8}{\pi^2} R_L \cdot \sum_{i=1}^{n} \left(M_i \cdot \prod_{j=1, j\neq i}^{n} Z_j \right)}{Q}$$

$$P_s = \mathrm{Re}\left\{ U_s \cdot I_s \right\} = \mathrm{Re}\left\{ \frac{\omega^2 U_{\mathrm{AC}}^2 \cdot Z_n \cdot \left(\sum_{i=1}^{n} \left(M_i \cdot \prod_{j=1, j\neq i}^{n} Z_j \right) \right)^2}{Q^2} \right\}$$

$$P_p = \mathrm{Re}\left\{ U_{\mathrm{AC}} \cdot I_p \right\} = \mathrm{Re}\left\{ \frac{U_{\mathrm{AC}}^2 \cdot \left(\sum_{i=1}^{n+1} \prod_{j=1, j\neq i}^{n+1} Z_j \right)}{Q} \right\}$$

$$\eta = \frac{P_s}{P_P} = \mathrm{Re}\left\{ \frac{\omega^2 Z_n \cdot \left(\sum_{i=1}^{n} \left(M_i \cdot \prod_{j=1, j\neq i}^{n} Z_j \right) \right)^2}{Q \cdot \left(\sum_{i=1}^{n+1} \prod_{j=1, j\neq i}^{n+1} Z_j \right)} \right\} \times 100\%$$

$$Q = \omega^2 \sum_{i=1}^{n} M_i^2 \cdot \prod_{j=1, j\neq i}^{n} Z_j + Z_p \cdot \sum_{i=1}^{n+1} \prod_{j=1, j\neq i}^{n+1} Z_j + \frac{1}{2}\omega^2 \sum_{i=1, j=1, i\neq j}^{n} \left((M_i - M_j)^2 \cdot \prod_{l=1, l\neq i, l\neq j}^{n+1} Z_l \right) \quad (6)$$

when $n = 1$, there is a particular solution

$$I_p = \frac{U_{\mathrm{AC}} (Z_1 + Z_2)}{\omega^2 M_1^2 + (Z_1 + Z_2) Z_p}$$

$$I_1 = \frac{-j\omega M_1 U_{\mathrm{AC}}}{\omega^2 M_1^2 + (Z_1 + Z_2) Z_p}$$

$$I_s = \frac{-j\omega M_1 U_{\mathrm{AC}}}{\omega^2 M_1^2 + (Z_1 + Z_2) Z_p}$$

$$U_s = \frac{-j\omega M_1 U_{\mathrm{AC}} \cdot \frac{8}{\pi^2} R_L}{\omega^2 M_1^2 + (Z_1 + Z_2) Z_p}$$

$$P_s = \mathrm{Re}\left\{ U_s \cdot I_s \right\} = \mathrm{Re}\left\{ \frac{\omega^2 M_1^2 U_{\mathrm{AC}}^2 Z_2}{\left(\omega^2 M_1^2 + (Z_1 + Z_2) Z_p \right)^2} \right\}$$

$$P_p = \mathrm{Re}\left\{ U_{\mathrm{AC}} \cdot I_p \right\} = \mathrm{Re}\left\{ \frac{U_{\mathrm{AC}}^2 (Z_1 + Z_2)}{\omega^2 M_1^2 + (Z_1 + Z_2) Z_p} \right\}$$

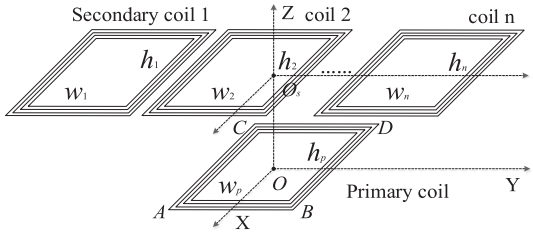

Fig. 3. Schematic diagram of the one-to-many multicoil model.

$$\eta = \frac{P_s}{P_P} = \mathrm{Re}\left\{ \frac{\omega^2 M_1^2 Z_2}{\left(\omega^2 M_1^2 + (Z_1 + Z_2) Z_p \right) (Z_1 + Z_2)} \right\} \times 100\% \quad (7)$$

where P_P and P_S are the input power and load power of the system, respectively, and η is the transfer efficiency of the system.

III. Simulation of the Proposed System

When the EVs or RVs enter the positioning area, the schematic diagram of the model is shown in Fig. 3, where the lengths and widths of the primary coil are w_p and h_p, and these values for the secondary coils are $w_1, \ldots, w_n$ and $h_1, \ldots, h_n$, respectively. The points O and O_s are the geometrical centers of the primary coil and the secondary coil pack, respectively.

A. Secondary Coils Control Strategy Simulation

An analytical calculation of the mutual inductance of the coaxial spiral rectangular coils is introduced in [11]. The method is extended to calculate the mutual inductance of parallel misaligned solenoid rectangular coils in [6]. The mutual inductance caused by the primary coil over the secondary coil can be expressed by

$$M = \sum_{i=1}^{N_1} \sum_{j=1}^{N_2} \begin{pmatrix} \Phi_{AB\_Z}(i,j) + \Phi_{BC\_Z}(i,j) \\ + \Phi_{CD\_Z}(i,j) + \Phi_{DA\_Z}(i,j) \end{pmatrix} \quad (8)$$

where N_1 and N_2 are turns of the two coils. $\Phi_{AB\_Z}(i,j)$ is the magnetic flux generated in the Z-axis direction to the *jth* turn of the receiving coil when 1 A RMS current flows on the *ith* turn of the primary coil; the other notations $\Phi_{BC\_Z}(i,j)$, $\Phi_{CD\_Z}(i,j)$, and $\Phi_{DA\_Z}(i,j)$ in the formula are similarly defined.

For simulating the actual situation, a one-to-multiple WPT MATLAB model with four secondary coils is built. In the model, the length and width of each coil are, respectively, 240 and 180 mm, and the turns number is 17. The vertical gap is 40 mm, and horizontal displacement between O and O_s is -720 to 720 mm. According to (8), the mutual inductances between the primary coil and each secondary coil calculated by MATLAB are shown in Fig. 4.

As to WPT systems, energy is exchanged through coils between those tightly coupled [6]. For example, when the primary coil is centered around the second secondary coil (from 85 to 155 mm), M_2 is much larger than M_1, M_3, and M_4, meaning that the received power of the first, third, and fourth coils is small

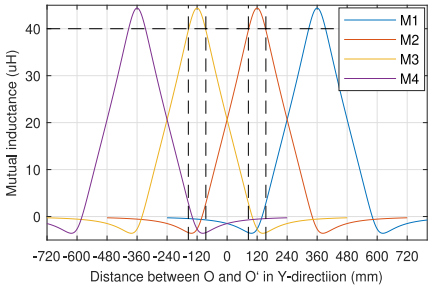

Fig. 4. Mutual inductance between the primary coil and each secondary coil.

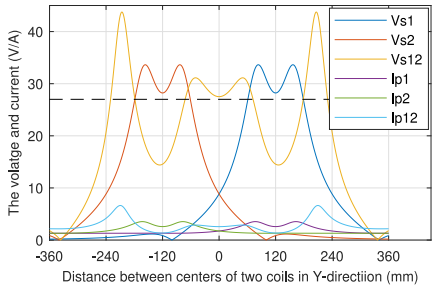

Fig. 5. Simulation of load voltage and primary current.

TABLE I
PARAMETERS FOR SIMULATION

symbol	parameter	value
U_{DC}	DC input voltage	30 V
f	Self-resonant frequency	85 kHz
L_p	Resonant inductance of the primary coil	125 μH
L_1	Resonant inductance of the 1st secondary coil	125 μH
L_2	Resonant inductance of the 2nd secondary coil	125 μH
C_p	Resonant capacitance of the primary loop	28 nF
C_1	Resonant capacitance of 1st secondary loop	28 nF
C_2	Resonant capacitance of 2nd secondary loop	28 nF
R_p	Parasitic resistance of the primary loop	0.1 Ω
R_1	Parasitic resistance of 1st secondary loop	0.1 Ω
R_2	Parasitic resistance of 2nd secondary loop	0.1 Ω
R_s	Parasitic resistance of the load loop	0.1 Ω
R_L	Load resistance	10 Ω

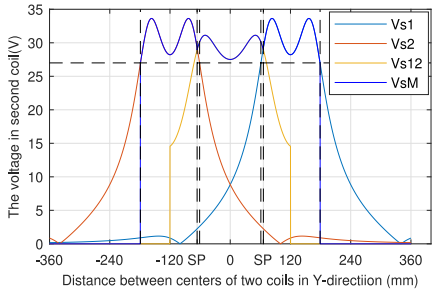

Fig. 6. Simulation of load voltage.

and can be ignored to simplify the analysis. At the same time, the first, third, and fourth secondary loop can be closed to reduce loop losses. In other words, in the range where M_2 is much larger than the value 40 μH while the others are quite small, then M_1, M_3, and M_4 can be ignored. Besides, in another range for example from -85 to 85 mm, although M_2 and M_3 themselves are not so large but still much larger than M_1 and M_4, the system can still transmit significant power, as analyzed in Section II, so M_1 and M_4 can be ignored and the first and fourth secondary loop can be closed. The abovementioned analysis shows that only one or two secondary coils are need to effectively transmit power. So, only a two-coil system is considered in the following section.

B. Circuit Simulation

The parameters for the simulations of a one-to-two system are listed in Table I. For this system, I_p and U_s can be computed as in (6). Fig. 5 depicts the wireless power transmission characteristics of the one-to-two WPT system, by moving the secondary coil pack from -360 to 360 mm. For Fig. 5, when only the ith ($i = 1$ or 2) secondary coil is switched ON, load voltage and current of the primary loop are denoted as V_{si} and I_{pi}, respectively. When both secondary coils are turned ON at the same time, V_{s12} is the load voltage, and I_{p12} is the current in the primary loop.

It is evident that V_{s12} has two peaks, which cause I_{p12} to increase. Additionally, the increase in I_{p12} will produce more heat in MOSFETs and will make the inverter prone to failure. Therefore, the system should be turned OFF to protect the equipment from damage in the two peaks. After the two peaks are skipped, the voltage of the load is shown in the Fig. 6.

To ensure the continuity of the load voltage and make the load voltage as high as possible, the threshold voltage of the load can be selected, for example, as 27 V. In Fig. 6, it can be observed that the positioning area with a single secondary coil is 118 mm (61 to 179 mm with coil 1 or -179 to -61 mm with coil 2). With the moving of the secondary coil pack, the use of a single secondary coil cannot make the load voltage exceed the threshold voltage in the area between the two coils (-61 to 61 mm). Fortunately, if the two secondary coils are working at the same time, the load voltage will exceed the threshold voltage. This working mode that allows for an adjustable number of secondary coils to work is called the mixed mode. For the mixed mode where a single secondary coil or double secondary coils can be used, the positioning area can be expanded to 358 mm (-179 to 179 mm), as shown by V_{sM} in Fig. 6. The points of 66 and -66 mm in X-axis are switching points (SPs) where the system switches from the single coil mode to the mixed mode. The positioning range of two coils in mixed mode is obviously much larger than the case of a single coil. Needless to say, if there are more secondary coils, the positioning area can be further enlarged.

Fig. 7 is the system transmission efficiency of the one-to-two simulation model. η_i is the system efficiency when only the ith ($i = 1$ or 2) secondary coil is switched ON. When both secondary coils are turned ON at the same time, η_{12} is the system efficiency. For the mixed mode where a single secondary coil or double secondary coils can be used, the system efficiency is denoted by η_M. According to the η_M in Fig. 7, it can be seen that when the EVs park at any point in the positioning area of -179 to 179 mm

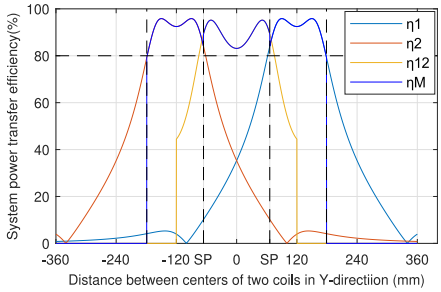

Fig. 7. Simulation of system efficiency.

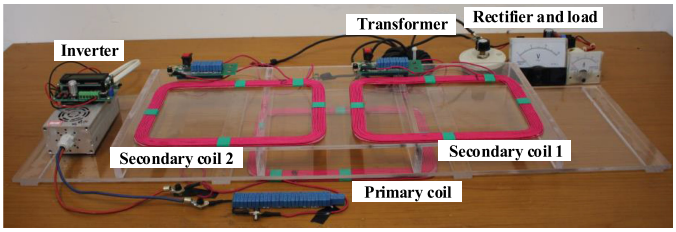

Fig. 8. Fabricated one-to-two WPT system prototype.

TABLE II
PARAMETERS FOR THE VERIFICATION SYSTEM

symbol	parameter	value
U_{DC}	DC input voltage	30 V
f	Self-resonant frequency	85 kHz
L_p	Resonant inductance of the primary coil	139.66 μH
L_1	Resonant inductance of the 1st secondary coil	140.95 μH
L_2	Resonant inductance of the 2nd secondary coil	140.28 μH
C_p	Resonant capacitance of the primary loop	24.97 nF
C_1	Resonant capacitance of 1st secondary loop	24.74 nF
C_2	Resonant capacitance of 2nd secondary loop	24.59 nF
R_p	Parasitic resistance of the primary loop	0.220 Ω
R_1	Parasitic resistance of 1st secondary loop	0.197 Ω
R_2	Parasitic resistance of 2nd secondary loop	0.201 Ω
R_s	Parasitic resistance of the load loop	0.027 Ω
R_L	Load resistance	10 Ω

shown in Fig. 6, the power transmission efficiency of the system is no less than 80%.

IV. PROTOTYPE AND EXPERIMENT

For verification, a WPT system with two secondary coils were fabricated. Fig. 8 depicts the one-to-two WPT system with a three winding transformer. Each planar solenoid coils are a rectangle of 240 mm × 180 mm. All coils, containing 17 turns, are made of Litz wire, which includes 1200 isolated strands with an outer diameter of 2.43 mm. The diameter of each strand is 0.01 mm, and the vertical air gap is 40 mm. The distance between the centers of the two secondary coils is 270 mm. In the case, the mutual inductance between the two secondary coils is only 4.36 μH, which is much smaller than the mutual inductances between the primary coil and each secondary coil. A full-bridge rectifier is built at the secondary side and the load is 10 Ω. The main parameters are listed in Table II, where the resistances, inductances, and capacitances are measured by the

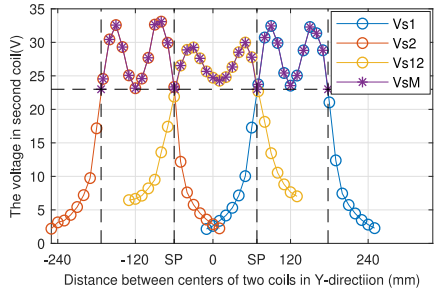

Fig. 9. Experimental results of load voltage.

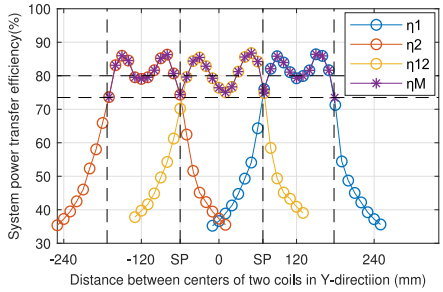

Fig. 10. Experimental results of system efficiency.

Agilent E4980 A LCR meter at 85 kHz. The experimental results are shown in Fig. 9.

To measure the load voltage when the secondary coils are packed in different positions, the secondary side moves intermittently at 10 mm intervals. For the single coil mode, the load voltage curves of coils 1 and 2 are denoted as V_{s1} and V_{s2}, respectively. Under the mixed mode, the load voltage is V_{s12}. To ensure the continuity of the load voltage, 23 V is selected as the threshold voltage. In Fig. 9, it can be seen that under the single mode, the positioning range of coil 1 is 110 mm (178 to 68 mm) and coil 2 is 113 mm (−173 to −60 mm). Meanwhile, if −60 and 68 mm are selected as the SPs, the positioning range of the mixed mode can be expanded to 351 mm (−173 to –178 mm), as shown by V_{sM}. The threshold voltage of the experiment is lower than that in the simulation model, on the one hand, there are some inevitable deviations between test and simulation parameters, on the other hand, the power losses have not been taken into account in the simulation model. Fortunately, the experimental data are consistent with the trend of the simulation model, which verifies that the one-to-multiple topology can effectively expand the positioning range. Fig. 10 is the system efficiency of the one-to-two WPT system. For the single coil mode, the system efficiency of coils 1 and 2 are denoted as η_1 and η_2, respectively. Under the mixed mode, the system efficiency is η_{12}. For the mixed mode, the system efficiency is denoted by η_M. The curve in Fig. 10 shows that the power transmission efficiency of the system is no less than 73.5% and actually more than 80% in most areas at the power level of 50 W when the EVs park at any point in the positioning area of −173 to 178 mm. The trend of the system efficiency experiment results is basically consistent with the simulated results. As some losses are not considered

in the simulated model, the experimental results of the system efficiency are slightly lower than the simulated ones.

V. Conclusion

In this letter, a new one-to-multiple WPT system for free positioning has been proposed. The system is interpreted through circuit analysis and experimentally verified by a fabricated WPT system with two secondary coils. The multiwinding transformer is used to solve the power integration problem in the case of multiple secondary coils, and the energy transmission characteristics of multiple secondary coils are investigated through circuit analysis. In order to achieve the goal of free positioning, a mixed operation mode is proposed, which allows the positioning range of EVs or RVs to be arbitrarily expanded. Experiments show that two secondary coils in the mixed mode can expand the positioning range by about three times compared to the one coil case.

References

[1] Y. Li, Y. Sun, and X. Dai, "/spl mu/-synthesis for frequency uncertainty of the ICPT system," *IEEE Trans. Ind. Electron.*, vol. 60, no. 1, pp. 291–300, Jan. 2013.

[2] Y. Li, R. Mai, L. Lu, and Z. He, "A novel IPT system based on dual coupled primary tracks for high power applications," *J. Power Electron.*, vol. 16, no. 1, pp. 111–120, 2016.

[3] J. M. Miller and A. Daga, "Elements of wireless power transfer essential to high power charging of heavy duty vehicles," *IEEE Trans. Transp. Electrific.*, vol. 1, no. 1, pp. 26–39, Jun. 2015.

[4] J. H. Kim *et al.*, "Development of 1-MW inductive power transfer system for a high-speed train," *IEEE Trans. Ind. Electron.*, vol. 62, no. 10, pp. 6242–6250, Oct. 2015.

[5] D. Kurschner and C. Rathge, "Integrated contactless power transmission systems with high positioning flexibility," in *Proc. 13th Int. Power Electron. Motion Control Conf.*, Sep. 2008, pp. 1696–1703.

[6] Q. Deng *et al.*, "Edge position detection of on-line charged vehicles with segmental wireless power supply," *IEEE Trans. Veh. Technol.*, vol. 66, no. 5, pp. 3610–3621, May 2017.

[7] J. L. Villa, J. Sallan, J. F. Sanz Osorio, and A. Llombart, "High-misalignment tolerant compensation topology for ICPT systems," *IEEE Trans. Ind. Electron.*, vol. 59, no. 2, pp. 945–951, Feb. 2012.

[8] J. W. Kim *et al.*, "Wireless power transfer for free positioning using compact planar multiple self-resonators," in *Proc. IEEE MTT-S Int. Microw. Workshop Ser. Innovative Wireless Power Transmiss.: Technologies, Syst., Appl.*, May 2012, pp. 127–130.

[9] J. Cheng, J. Shi, and X. He, "A novel input-parallel output-parallel connected DC-DC converter modules with automatic sharing of currents of different resonant frequencies," in *Proc. 7th Int. Power Electron. Motion Control Conf.*, 2015, pp. 6001–6005.

[10] Y. Zhang, T. Lu, Z. Zhao, F. He, K. Chen, and L. Yuan, "Selective wireless power transfer to multiple loads using receivers of different resonant frequencies," *IEEE Trans. Power Electron.*, vol. 30, no. 11, pp. 6001–6005, Nov. 2015.

[11] Y. Cheng and Y. Shu, "A new analytical calculation of the mutual inductance of the coaxial spiral rectangular coils," *IEEE Trans. Magn.*, vol. 50, no. 4, Apr. 2014, Art. no. 7026806.